Eur. J. Mineral., 38, 123–134, 2026
https://doi.org/10.5194/ejm-38-123-2026

European Journal of Mineralogy
Open Access

High-spatial-resolution oxygen isotopic analysis to distinguish natural from synthetic corundum

Elena S. Sorokina[1], Axel K. Schmitt[2,3], Tobias Häger[4], and Jens Hopp[3]

[1]Vernadsky Institute of Geochemistry and Analytical Chemistry, Russian Academy of Sciences, 119991 Moscow, Russia
[2]John de Laeter Centre, Curtin University, Bentley WA 6102, Australia
[3]Institut für Geowissenschaften, Universität Heidelberg, 69120 Heidelberg, Germany
[4]Insitut für Geowissenschaften, Johannes Gutenberg-Universität Mainz, 55099 Mainz, Germany

Correspondence: Elena S. Sorokina (esorokina@geokhi.ru) and Tobias Häger (haeger@uni-mainz.de)

Received: 28 August 2025 – Revised: 2 February 2026 – Accepted: 20 February 2026 – Published: 18 March 2026

Abstract. Gem-quality corundum varieties of ruby and sapphire are one of the most valuable and desired gemstones. Due to their rarity, new methods of synthesis and treatment were developed over the last decades, complicating the reliable identification between natural, treated, and synthetic specimens. Among the geochemical methods used for identification, trace element analysis using laser ablation inductively coupled plasma mass-spectrometry (LA-ICP-MS) is widely applied. However, solely relying on LA-ICP-MS trace element analysis for differentiation between natural and synthetic corundum origins, especially when grown by the hydrothermal method, can potentially lead to misidentifications. To further enable geochemical tracing of corundum, this study explores secondary ion mass spectrometry (SIMS) oxygen isotope analysis. High-spatial-resolution SIMS δ^{18}O analysis of hydrothermally synthesized corundum yielded values between -7.84 ± 0.13 ‰ and -14.54 ± 0.13 ‰ (relative to Vienna standard mean ocean water, VSMOW; 1 standard error) that are atypical for natural corundum. For flame fusion corundum, SIMS δ^{18}O analyses are in the range of -6.73 ± 0.13 ‰ to -17.46 ± 0.13 ‰ for sapphires of blue, yellow, and orange colour and $+28.51 \pm 0.11$ ‰ to $+30.47 \pm 0.10$ ‰ for ruby, which, in both cases, are again atypical for natural corundum. SIMS δ^{18}O analysis of corundum thus has strong potential to distinguish synthetic and natural corundum.

1 Introduction

Gem-quality corundum varieties, ruby and sapphire, are, after diamond, the most important gemstones from a commercial standpoint and account for more than 50 % of global coloured-gem production (Hughes, 2017). Their value results from high demand paired with rare large-scale commercial deposits. Only about 15 occurrences worldwide produce ruby and sapphire suitable for facetting or cabochoning (Giuliani et al., 2014; Hughes, 2017). Due to the rarity of gem corundum, new methods of its synthesis and treatment were developed over the last decades, and it is very rare to find gem corundum on the market that has not been treated (Giuliani and Groat, 2019). Hydrothermal synthesis in particular can produce synthetic corundum with properties very similar to their natural counterparts (Schmetzer and Peretti, 1999), which challenges their identification. In the light of an unabatedly high demand for ruby and sapphire, devising analytical methods to identify gem origins that are ideally non-destructive or only minimally destructive is an important goal not only for mineralogy and gemology but also for forensic science.

Almost all physical features (refractive indices, density, etc.) of synthetic corundum are similar to their natural analogues. Therefore, over the last decades, the most prominent non-destructive method applied for the distinction between synthetic and natural corundum remained optical microscopy targeting internal features such as solid inclusions within gem corundum (Gubelin and Koivula, 1997). Moreover, breakthroughs in studying gem corundum chemistry

have been accomplished over the last 30 years with the development of modern analytical methods. Currently many geochemical fingerprinting schemes have been devised for rubies and sapphires from different origins but also to identify synthetic counterparts (e.g. Muhlmeister et al., 1998; Peucat et al., 2007). Muhlmeister et al. (1998) applied energy-dispersive X-ray fluorescence (EDXRF) to point out the absence of Ga in synthetic corundum as a distinguishing feature compared to natural analogues (Muhlmeister et al., 1998). However some synthetic stones can still contain Ga if analysed by more sensitive instrumentation such as laser ablation inductively coupled plasma mass spectrometry (LA-ICP-MS; current research). Palke and Shigley (2024) also indicated that the finding of Ga by means of LA-ICP-MS within some hydrothermally synthesized corundum complicated the identification process.

LA-ICP-MS features lower detection limits than EDXRF. It also does not require extensive sample preparation such as conductive coating or transfer into vacuum and, hence, can be applied even for cut stones. Therefore, LA-ICP-MS has been used widely in gemology since the beginning of this millennium (Breeding et al., 2010).

Among spatially selective analysis methods, secondary ion mass spectrometry (SIMS) has higher sensitivity compared to LA-ICP-MS, allowing trace element analysis in a smaller sample volume (see Fig. 1). Moreover, SIMS spot analysis can determine oxygen isotope ratios, whereas interferences in the Ar plasma gas, atmospheric contributions, and low ionization efficiency prevent meaningful isotopic analysis by LA-ICP-MS (Liu et al., 2025). This has tremendous potential to trace genetic and geographic provenance through the determination of $\delta^{18}O$ in naturally occurring corundum (e.g. Giuliani et al., 2014; Wong and Verdel, 2017; Sorokina et al., 2021; Schmidt et al., 2024). Pioneering studies analysed $\delta^{18}O$ in hydrothermally synthesized and flux-grown corundum by gas source mass spectrometry and thus required powder preparation, which is detrimental for gem-quality materials (Pomian-Srzednicki, 1997; Bidny et al., 2010). Moreover, results can be compromised by incorporating inclusions into the analysis powder. Here, we explore high-spatial-resolution SIMS $\delta^{18}O$ analysis of synthetic and treated rubies and sapphires with minimal sample destruction. The obtained results are promising for their application in differentiating between natural and synthetic stones for gemology and mineralogy.

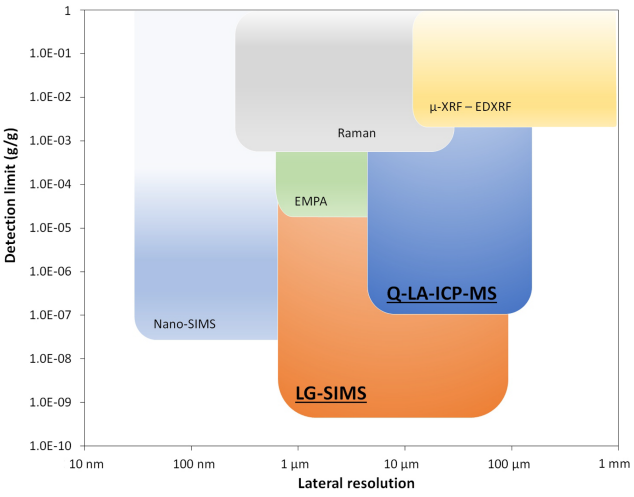

Figure 1. Diagram demonstrating analytical limitations (detection limits in $g\,g^{-1}$ – y axis; spatial resolution – x axis) for some microbeam technique applied for the investigation and origin determination of gemstones in different time periods, as modified from Li and Li (2016). EMPA: electron micro-probe analysis; μ-XRF: micro-X-ray fluorescence; EDXRF: energy dispersive X-ray fluorescence; Q-LA-ICP-MS: quadrupole LA-ICP-MS.

2 Material and methods

2.1 Sample strategy

We studied nine treated (five Be-diffused yellow samples and two high-temperature (HT) treated pairs from pale-blue to blue colour) and 16 differently coloured synthetic corundum crystals grown by flame fusion (number $n = 8$), Czochralski ($n = 1$), and hydrothermal ($n = 7$) methods. Synthetic samples were directly obtained from manufactures, whereas HT pairs were collected after colour change (colourless to blue) which was induced by heating experiments at 1700 °C in a chamber furnace in a non-controlled atmosphere (open corundum crucible in air). Be-diffused samples were treated in the same furnace at 1700 °C during 50 h in a closed crucible, and the samples were embedded in chrysoberyl ($BeAl_2O_4$) powder. Ruby from Karelia (Russia) from the collection of Johannes Gutenberg-Universität Mainz (JGU) was also analysed by SIMS in order to verify the values for the only known naturally occurring corundum strongly depleted in $\delta^{18}O$. Samples were cut to millimetre-wide wafers, arranged on adhesive tape and embedded into epoxy resin to minimize sample changes (Fig. 2), but we emphasize that cut gemstones can also be directly mounted in a SIMS sample holder (e.g. Giuliani et al., 2000; Wang et al., 2018). After sectioning and polishing with abrasives up to 1 µm diamond suspension, the mounts were ultrasonically cleaned with deionized water and ethanol.

To better constrain the causes of heterogeneous $\delta^{18}O$ values for the two different Be-diffused materials studied here, we performed dedicated Be diffusion experiments under controlled conditions. For this, corundum samples originating from magmatic and metamorphic sources were selected since they have distinctly different oxygen isotopic compositions, with approximate $\delta^{18}O$ values of +5.5 ‰ for magmatic and between +14 ‰ and +25 ‰ for metamorphic sources (Wong and Verdel, 2017). Two stones of magmatic (average $\delta^{18}O = 6.45$ ‰ and 6.28 ‰) and two stones of metamorphic (average $\delta^{18}O = 13.28$ ‰ and 15.80 ‰) origins were cut into

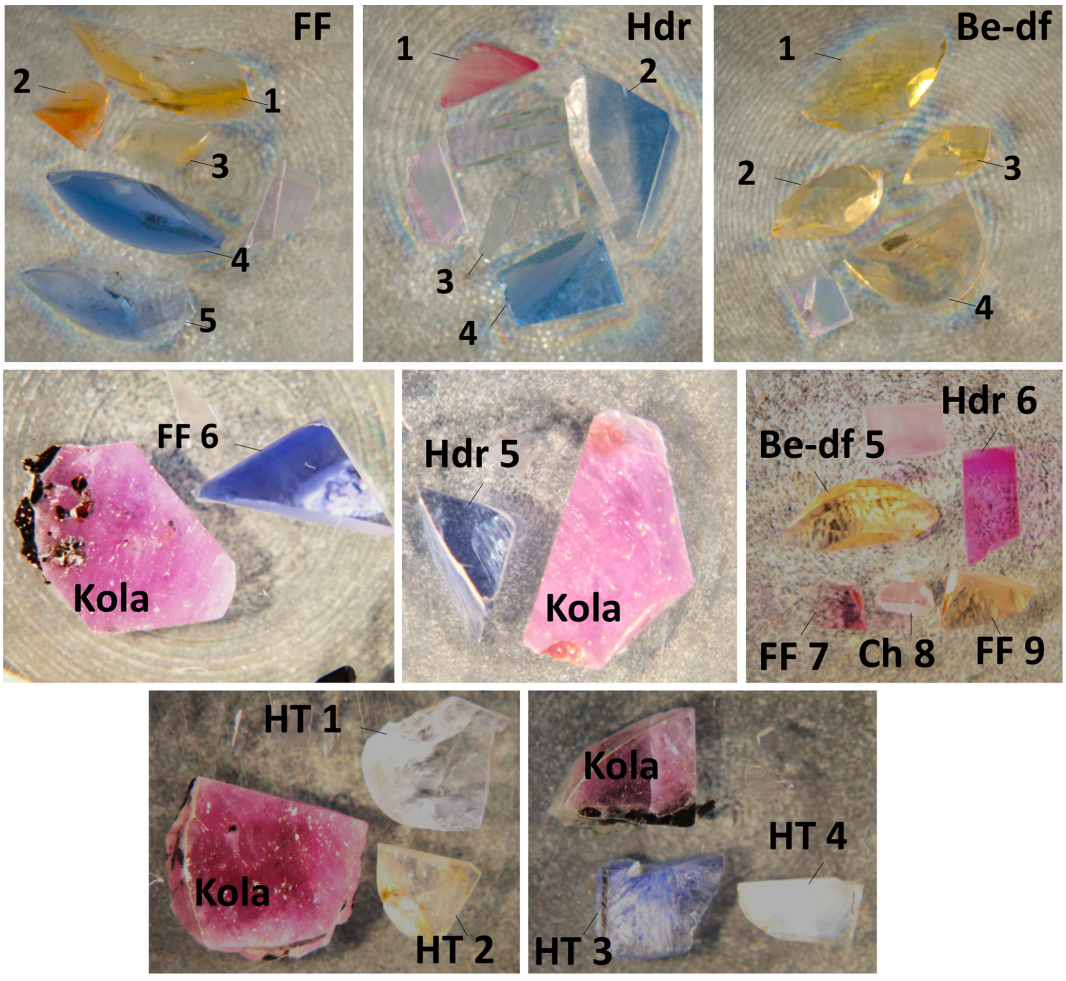

Figure 2. Optical image of treated corundum samples (Be diffusion (Be df) and high temperature (HT) treatment) along with synthetic material (flame fusion (FF) and hydrothermal (Hdr) methods) used in this study. The number of samples and their dimensions are given in Tables 1–3. Kola: Karelian corundum; Ch: Czochralski-grown corundum.

two pieces, where one piece of each stone was further Be diffused by a gem manufacturer at 1700 °C over 50 h.

2.2 Laser ablation inductively coupled plasma mass spectrometry (LA-ICP-MS)

Before LA-ICP-MS trace element measurements, optical microscopic inspection was carried out in order to avoid areas with inclusions and to identify internal features such as colour zonation. LA-ICP-MS analysis of heat-treated, Be-diffused, and synthetic corundum was applied to determine their trace element composition by using an ESI NWR193 ArF Excimer Laser combined with an Agilent 7500ce quadrupole-ICP-MS at the Institut für Geowissenschaften, JGU, Germany. The samples were ablated with a spot size of 70 µm. The repetition rate was 10 Hz, and the energy density was approximately 3.3 J cm^{-2} during the measurements. Every spot was analysed with 50 s warmup/background time, 30 s dwell time, and 20 s wash-out time. Trace elements of interest within the corundum samples included the following isotopes: ^{24}Mg, ^{47}Ti, ^{51}V, ^{52}Cr, ^{56}Fe, ^{60}Ni, and ^{71}Ga. Other masses including ^{6}Li, ^{9}Be, ^{23}Na, ^{29}Si, ^{39}K, ^{43}Ca, ^{55}Mn, ^{88}Sr, ^{90}Zr, ^{93}Nb, ^{137}Ba, ^{179}Hf, ^{181}Ta, and ^{208}Pb were added to monitor contamination with solid inclusions in time-resolved spectra but also to assess the impact of the Be-diffusing process as applied to some of the treated material. NIST SRM 610 glass was used as the primary reference material (Jochum et al., 2005, Jochum et al., 2011), and NIST SRM 612, USGS BCR-2G, USGS GSD-1G, and USGS GSE-1G glasses were used as quality control materials. Reference and quality control materials were measured after sets of 30 unknown corundum samples to monitor the accuracy and precision of calibration. The time-resolved signal spectra were processed in GLITTER 4.4.1 software (http://www.glitter-gemoc.com, last access: March 2026, Macquarie University, Sydney, Australia) using ^{27}Al as the internal standard, applying a theoretical value of Al_2O_3 at 100 wt % for the corundum samples and

values given in the GeoReM database for the reference material. The measured concentrations for both QCM (quality-control material) agree for most trace elements of interest and were less than 15 % of the preferred values provided in the GeoReM database.

2.3 Secondary ion mass spectrometry (SIMS) of oxygen isotopes

The oxygen isotope composition of the same corundum crystals analysed previously by LA-ICP-MS was determined using CAMECA IMS1280-HR and IMS 1300-HR3 ion microprobes at Heidelberg University (HIP) in Germany and at Curtin University (John de Laeter Center) in Australia, respectively. Before the SIMS measurements, BSE (backscattered electron) images were taken using a LEO 440 scanning electron microscope coupled with an Oxford Instruments X-Max energy dispersive spectrometer in order to avoid areas with inclusions. The surface was then cleaned and coated with a $\sim$ 50–80 nm thick conductive Au layer. An $\sim$ 2 nA and 20 keV total impact energy Cs^+ primary ion beam with a raster size of 10 µm (12 µm during pre-sputtering) was used for rim-to-rim measurements of corundum, avoiding direct proximity to the LA-ICP-MS craters. Sample charging was compensated for with a normal incidence electron gun, and negative secondary ions were accelerated to a kinetic energy of 10 keV. The ^{16}O and ^{18}O secondary ion beams were detected simultaneously in two Faraday cups with a mass resolving power of $\sim$ 2300 (m Δm^{-1} at 10 % peak height). Prior to each analysis, the secondary beam was centred automatically in the field aperture (X and Y) and the entrance slit (X only). Including the time for beam centring, the analyses started after a total pre-sputtering time of 90 s, and each analysis had 20 cycles with 4 s integration time per cycle. The baseline of the FC amplifiers was determined with an integration time of 200 s or as a running average of 7×30 s integrations. The internal precision reported is the standard deviation of the mean value of the isotope ratios. The instrumental mass fractionation (IMF) was determined using HD-LR1, a synthetic laser ruby ($\delta^{18}O = +18.40 \pm 0.14$ ‰, 95 % confidence internal; Schmidt et al., 2024) placed on the same mount as the samples (all $\delta^{18}O$ values relative to Vienna Standard Mean Ocean Water (SMOW) with $^{18}O/^{16}O = 0.0020052$; Baertschi, 1976). Bracketing analyses of HD-LR1 indicate a repeatability of the IMF of between 0.08 and 0.16 ‰ (1 SD) on individual mounts and 0.36 ‰ (1 SD) between different mounts. In the absence of a secondary corundum reference, reference zircon AS3 and 91500 were analysed under the same instrumental settings, and, when using 91500 as the primary reference ($\delta^{18}O = 9.86$ ‰; Wiedenbeck et al., 2004), a value of $+5.40 \pm 0.01$ ‰ ($n = 7$) was obtained, which agrees closely with the reported composition of +5.34 ‰ (Trail et al., 2007).

3 Results

3.1 LA-ICP-MS measurements

Trace elements commonly found in corundum (Be, Mg, Ti, Fe, Cr, V, Ga, Ni) and applied for the identification of synthetic corundum material from natural and/or treated counterparts (Muhlmeister et al., 1998) were determined in 86 spots; one spot affected by irregular ablation, likely due to the presence of solid inclusions, was excluded from further consideration (Tables 1–3). Five yellow-coloured Be-diffused corundum samples were homogeneously enriched in Fe (up to 3720 µg g^{-1}) and also show a homogeneous distribution of Mg, V, Cr, and Ga with only minor fluctuations (Table 1). With the exception of one sample (no. 2 in Table 1), Ti abundances range from below the detection limit (bdl) to $\sim$ 100 µg g^{-1} likely due to ablation of micrometre-sized Ti-bearing minerals (ilmenite, rutile, etc.). Beryllium was also detected in these samples, reaching 13.7 µg g^{-1}. As in the case of Be-diffused samples, two HT pairs (colourless and blue-coloured) show a homogeneous distribution of Mg, V, Cr, and Ga. For the same pairs, Fe and Ti are heterogeneously distributed with abundances of up to 2300 and 339 µg g^{-1}, respectively. However, differences in trace element abundances between the colourless and HT-treated blue-colour parts of stone for a HT sample are insignificant.

Synthetic corundum samples are enriched by different chromophoric trace elements, depending on their colour. Accordingly, red- and orange-coloured varieties contain higher Cr values (max. 1.2 wt % in hydrothermally synthesized corundum) compared to other coloured or colourless samples. Chromium is mostly homogeneously distributed within flame fusion material, whereas abundances are heterogeneous within hydrothermally synthesized samples. Blue-coloured corundum samples yield higher Fe abundances (generally up to 536 µg g^{-1}, with one anomalous spot at 1540 µg g^{-1} of Fe within a colourless sample, likely due to ablation of an inclusion) and Ti (up to 555 µg g^{-1}) compared to the other coloured counterparts. Trace element variations indicate oscillatory zonation within hydrothermally synthesized samples, whereas such fluctuations are less obvious within flame fusion samples (Fig. 3). Magnesium and V are mostly homogeneously distributed within all studied synthetic materials, with minor variability. Gallium and Ni were also detected within synthetic sapphires. Although Ga was almost at the detection limit within flame fusion material, its content varies within the hydrothermally synthesized samples, reaching up to 63.2 µg g^{-1}. Nickel was detected in two blue-coloured hydrothermally synthesized sapphires reaching 2507 µg g^{-1}, but, for the rest of the hydrothermally synthesized material, it was below the detection limit. Czochralski-grown pink-coloured corundum is almost free of trace elements, except for Cr, which is present at abundances of 388–402 µg g^{-1}.

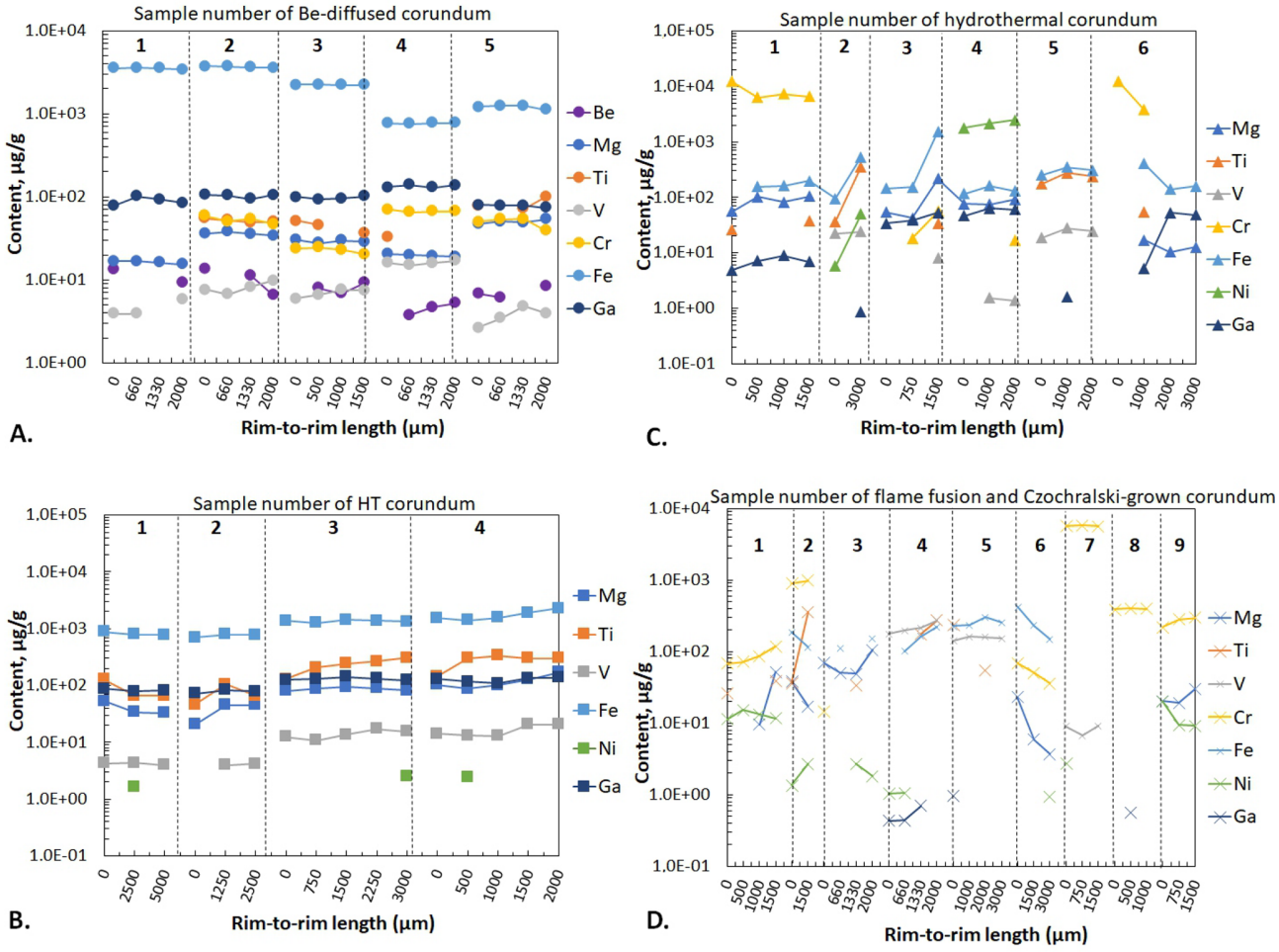

Figure 3. Distribution of trace elements (Mg, Ti, V, Cr, Fe, Ni, and Ga) within **(A)** Be-diffused corundum, **(B)** heat-treated (HT) corundum, **(C)** hydrothermally synthesized corundum, and **(D)** flame fusion and Czochralski-grown corundum.

3.2 SIMS measurements

In total, 450 points were analysed within the treated and synthetic corundum material, with all analyses showing identical secondary ion intensities as compared to reference corundum HD-LR1 (Tables 1–3). The results obtained on Be-diffused sapphires show both positive and negative oxygen isotopic compositions on the SMOW scale. Most Be-diffused sapphire samples ($n = 4$) yielded values around zero, with slightly negative or positive $\delta^{18}O$ variations from -0.90 ± 0.13 ‰ to $+0.58 \pm 0.11$ ‰; only one sample deviates to higher $\delta^{18}O$ values between $+12.81 \pm 0.12$ ‰ and $+13.21 \pm 0.12$ ‰.

Treated Be-diffused pieces of magmatic origin yielded $\delta^{18}O$ averages of 6.42 ‰ ($n = 10$) and 6.34 ‰ ($n = 10$), whereas treated pieces of metamorphic origin averaged 13.47 ‰ ($n = 10$) and 15.86 ‰ ($n = 10$) (Fig. 5). Thus, $\delta^{18}O$ values are indistinguishable between original and Be-diffused parts of these stones. The only exception is a yellow rim domain in a metamorphic Be-diffused crystal, where detailed SIMS mapping revealed a ~ 0.5 ‰ increase in $\delta^{18}O$ compared to the rest of the stone, whereas the untreated counterpart lacks this increase (Fig. 4).

The oxygen isotopic compositions of the HT-treated and HT-untreated pairs are similar: for the first pair, values range from $+14.21 \pm 0.08$ ‰ to $+14.55 \pm 0.10$ ‰, and, for the second pair, values range from $+15.74 \pm 0.15$ ‰ to 16.49 ± 0.16 ‰. Importantly, the HT-treated corundum crystals lack any significant $\delta^{18}O$ difference between the colourless and blue domains of the stone. One-way ANOVA tests performed on the two groups (original and HT-treated pieces) of the two stones analysed indicated p values of 0.4797 (samples 1 and 2, Table 1) and 0.0778 (samples 3 and 4, Table 1), which indicates that measured $\delta^{18}O$ values for original and HT-treated pairs are indistinguishable.

In contrast to natural corundum (with and without Be-diffusing and HT treatment), synthetic corundum generally displays strongly negative $\delta^{18}O$ values. This includes six hydrothermally synthesized samples with $\delta^{18}O$ values ranging

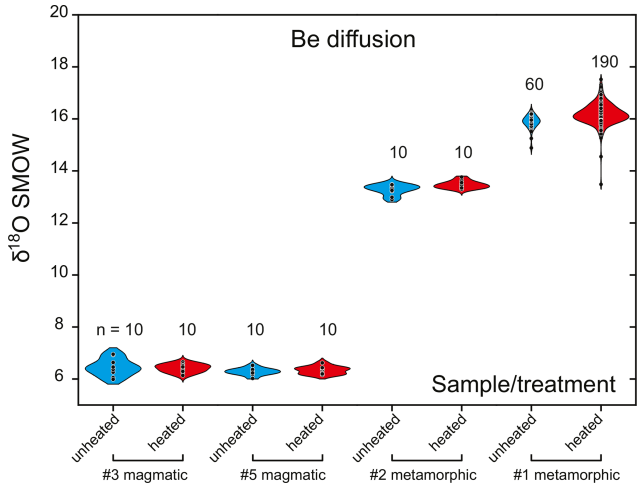

Figure 4. The $\delta^{18}O$ values of corundum samples used in Be-diffusing experiments.

from -7.89 ± 0.13 ‰ down to -14.54 ± 0.13 ‰ and seven flame fusion samples with $\delta^{18}O$ values between -6.73 ± 0.13 ‰ and -17.46 ± 0.13 ‰. The only exceptions are one red-coloured flame fusion sample and one Czochralski-grown sample: they yielded unusually high $\delta^{18}O$ values ranging from $+28.51 \pm 0.11$ ‰ to $+30.47 \pm 0.10$ ‰.

4 Discussion

4.1 LA-ICP-MS measurements

Different trace elements (Mg, Ti, Fe, Cr, Ga, etc.) and their ratios including Ga/Mg, Fe/Ti, Fe/Mg, and Cr/Ga are commonly used as a proxy for corundum origins (e.g. Peucat et al., 2007; Sutherland et al., 2009). However, some of these classification proxies are known to produce incorrect results, where, for example, ruby and sapphire compositions are convoluted (e.g. Palke et al., 2018; Sorokina et al., 2019; Filina et al., 2019; Wong and Verdel, 2017). Currently, the most reliable discrimination is based on the FeO–Cr_2O_3–MgO–V_2O_3 vs. FeO+TiO_2+ Ga_2O_3 diagram (Giuliani et al., 2014), which is applicable for both ruby and sapphire (Palke et al., 2018; Sorokina et al., 2019, etc.). This diagram is reproduced in Fig. 5 with new LA-ICP-MS data for treated and hydrothermally synthesized corundum of different colour varieties. Most of these data plot in the field of "metasomatic corundum" (Fig. 5). By contrast, ruby (red-colour varieties) data fall into the "ruby in marble" field. The reason why hydrothermally synthesized stones plot within the fields defined by naturally occurring corundum is likely due to the content of Ga in most of the hydrothermally synthesized corundum samples reaching up to 63.2 $\mu g\,g^{-1}$ (Table 2). Although Ni is present as a chromophore mostly in synthetic stones grown by the hydrothermal method (Schmetzer and Peretti, 1999), this cri-

Table 1. Rim-to-rim LA-ICP-MS and SIMS $\delta^{18}O$ analyses of high-temperature-treated and Be-diffused corundum samples.

No. of sample	Colour, size (mm)		LA-ICP-MS, ($\mu g\,g^{-1}$)							Ga/Mg	Fe/Ti	Cr/Ga	Fe/Mg	$\delta^{18}O$, (‰)	
		n*	Be	Mg	Ti	V	Cr	Fe	Ga					n	
Be-diffused															
1	Yellow 5 × 2	4	bdl–13.37 (5.65)	15.4–16.8 (16.1)	bdl	bdl –5.83 (3.4)	bdl	3410–3570 (3497)	84.4–101 (93)	4.7–6.0	–	–	211–221	4	+12.81 to +13.08 (+13.02)
2	Yellow 4 × 2	4	bdl–13.7 (7.88)	34.1–37.9 (36)	49.4–55.2 (51.7)	6.72–9.75 (8.09)	47–58.8 (52.6)	3570–3720 (3643)	94.3–106 (103)	2.6–3.1	67.4–72.7	0.4–0.6	97.3–105	4	+0.08 to +0.58 (+0.25)
3	Yellow 3 × 1.5	4	bdl–9.25 (6.03)	27.8–30.5 (29.2)	bdl–51.8 (33.55)	6.03–7.56 (6.91)	20.4–24.2 (23)	2210–2230 (2220)	93.1–102 (97)	3.2–3.6	0–60.1	0.2–0.3	73.1–80.2	4	−0.90 to −0.3 (−0.61)
4	Yellow 4 × 3	4	bdl–5.24 (3.44)	18.9–20.6 (19.8)	bdl–32.9 (8.22)	15–17 (16.1)	64.9–71 (67.5)	755–776 (769)	130–138 (135)	6.4–7.3	0–23.5	0.5	37.4–41	5	−0.33 to −0.15 (−0.25)
5	Yellow 5 × 2	4	bdl–8.37 (5.36)	47.5–53.7 (50.2)	bdl–100 (83.1)	2.66–4.83 (3.73)	39.1–54.3 (49.4)	1120–1250 (1208)	73.8–80.1 (78)	1.4–1.7	0–17.3	0.5–0.7	20.8–25.7	4	−0.35 to −0.21 (−0.26)
Heat-treated															
1	Blue 5 × 5	3	–	32.6–52.8 (39.7)	65.9–127 (86.3)	3.94–4.31 (4.16)	bdl	782–887 (818)	78.1–87.9 (82.6)	1.7–2.5	7–11.9	–	16.8–24	3	+14.21 to +14.43 (+14.35)
2	Colourless 3 × 2.5	3	–	20.6–44.9 (36.8)	46.2–106 (72.5)	bdl–4.19 (2.71)	bdl	694–790 (752)	72.1–82.6 (77.9)	1.8–3.5	7.5–15	–	17.2–33.8	3	+14.30 to +14.55 (+14.42)
3	Blue 4 × 3	5	bdl	80.5–94.6 (86.6)	130–309 (231)	10.9–17.1 (13.9)	bdl	1270–1440 (1366)	124–142 (131)	1.5–1.6	4.3–10.7	–	14.5–17.3	5	+15.85 to +16.49 (+16.23)
4	Colourless 4 × 2	5	bdl–2.3 (0.46)	87.1–171 (118)	144–339 (348)	13–20.5 (16.2)	bdl	1410–2300 (1746)	109–134 (126)	1.1–1.3	4.6–10.7	–	14.9–16.2	5	+15.74 to +16.10 (+15.98)

* n: number of spots or points; bdl: below the detection limit.

https://doi.org/10.5194/ejm-38-123-2026

Table 2. Rim-to-rim LA-ICP-MS and SIMS $\delta^{18}O$ analyses of hydrothermal corundum material.

No. of sample	Colour, size (mm)	LA-ICP-MS, ($\mu g\,g^{-1}$)								Ga/Mg	Fe/Ti	Cr/Ga	Fe/Mg	$\delta^{18}O$, (‰)	
		n*	Mg	Ti	V	Cr	Fe	Ni	Ga					n	
1	Red 3 × 1.5	4	56.1–105 (86.2)	26.2–38.2 (32.2)	bdl	6300–12 300 (8125)	bdl–197 (172)	bdl	4.88–8.88 (6.9)	0.07–0.11	0–5.15	822–2520	0–1.97	4	−12.20 to −11.53 (−11.92)
2	Blue-zonal 5 × 3	2	bdl	36.5–359 (198)	22.3–24 (23.2)	bdl	95.3–536 (316)	5.72–50 (28)	bdl–0.85 (0.9)	–	1.49–2.61	–	–	4	−14.54 to −12.10 (−13.21)
3	Colourless 3 × 1.5	3	53.9–216 (104)	bdl–33.7 (33.7)	bdl–8.08 (8.08)	bdl–56.3 (24.8)	146–1540 (613)	bdl	34.1–53.2 (42)	0.25–0.91	0–45.7	0–1.06	2.71–7.13	3	−10.34 to −9.37 (−9.94)
4	Blue 4 × 2	3	74.9–91.4 (80.9)	bdl	bdl–1.54 (1.5)	bdl–16.9 (5.6)	115–162 (136)	1790–2507 (2152)	46.4–63.2 (56.6)	0.61–0.84	0	0–0.28	1.43–2.16	4	−8.05 to −7.89 (−7.96)
5	Blue 3 × 2	3	bdl	175–273 (229)	18.5–28 (23.7)	bdl	250–349 (302)	bdl	bdl–1.6 (0.54)	–	1.28–1.43	–	–	3	−13.77 to −13.69 (−13.72)
6	Pink 3 × 1.5	4	bdl–16.9 (9.98)	bdl–54.7 (13.7)	bdl	bdl–12 400 (4050)	bdl–405 (141)	bdl	bdl–53.1 (26.6)	0–5.12	0–7.4	0–732	0–23.96	4	−13.98 to −9.37 (−11.83)

* n: number of spots or points; bdl: below the detection limit.

Table 3. Rim-to-rim LA-ICP-MS and SIMS $\delta^{18}O$ analyses of flame fusion and Czochralski-grown (Ch) corundum material.

No. of sample	Colour	LA-ICP-MS, ($\mu g\,g^{-1}$)								$\delta^{18}O$, (‰)	
		n	Mg	Ti	V	Cr	Fe	Ni	Ga	n	
1	Yellow 5 × 1.5	4	bdl–51.6 (15.3)	bdl	bdl	67.6–118 (86.1)	bdl	11.3–15.3 (12.9)	bdl	4	−7.19 to −6.73 (−6.90)
2	Orange 2 × 1.5	2	17–38.6 (27.8)	bdl	bdl	904–986 (945)	115–186 (151)	1.36–2.7 (2.0)	bdl	2	−9.88 to −9.80 (−9.84)
3	Yellow 2 × 1.5	4	49.3–106 (68.9)	bdl	bdl	bdl–14.8 (3.7)	bdl–151 (65.8)	bdl–2.71 (1.13)	bdl	4	−10.98 to −9.18 (−10.31)
4	Blue 6 × 2	4	bdl	112–555 (316)	176–272 (215)	bdl	bdl–222 (162)	bdl–1.06 (0.53)	bdl–0.7 (0.39)	4	−8.36 to −7.08 (−7.56)
5	Pale-blue 5 × 3	4	bdl	352–470 (400)	141–162 (154)	bdl	228–301 (255)	bdl	bdl–0.97 (0.24)	4	−9.02 to −8.16 (−8.58)
6	Blue 6 × 3	3	3.68–23	42.9–170 (92.6)	bdl	35.9–68.4 (51.6)	149–425 (268)	bdl–0.95 (0.24)	bdl	3	−9.84 to −8.52 (−9.23)
7	Red 1.5 × 1.5	3	bdl	bdl	6.72–9.13 (8.3)	5600–5800 (5700)	bdl	bdl–2.8 (0.7)	bdl	3	+28.51 to +29.28 (+28.88)
8	Ch*-Pink 1.5 × 1	3	bdl	bdl	bdl	388–402 (395)	bdl	bdl	bdl–0.57 (0.14)	3	+30.33 to +30.47 (+30.38)
9	Yellow 2 × 1.5	3	19.3–30.3	bdl	bdl	221–297 (266)	bdl	9.22–20.1 (12.9)	bdl	3	−17.46 to −16.84 (−17.09)

* Ch: Czochralski-grown corundum material; n: number of spots or points; bdl: below the detection limit.

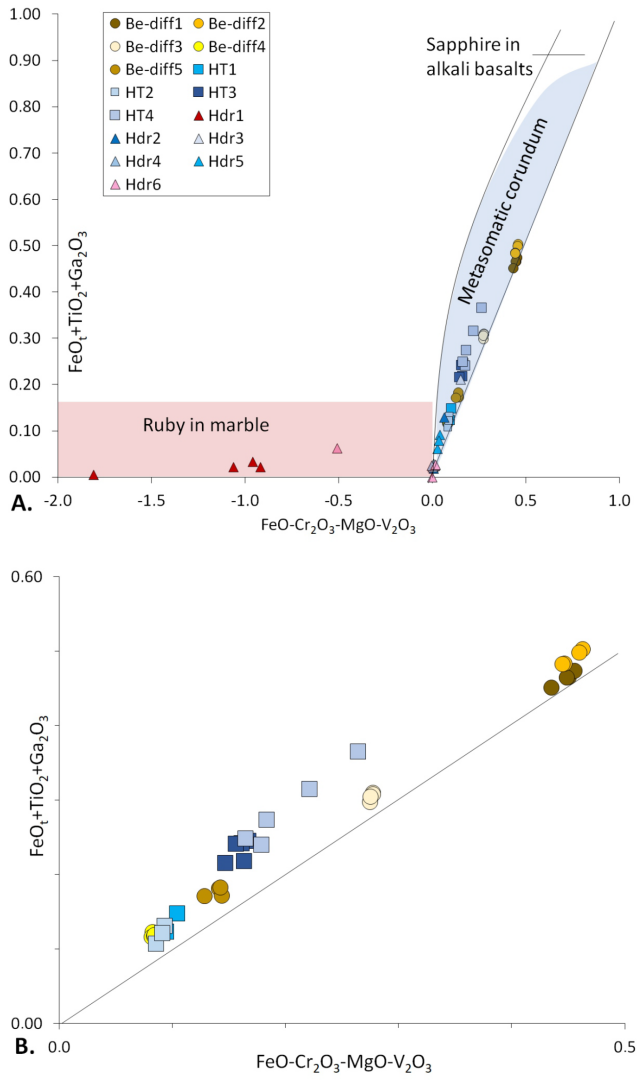

Figure 5. **(A)** The $FeO–Cr_2O_3–MgO–V_2O_3$ vs. $FeO+TiO_2+Ga_2O_3$ (wt %) provenance discrimination diagram by Giuliani et al. (2014) with trace element data on Be-diffused (Be-diff), HT-treated (HT), and hydrothermally synthesized corundum material. The number of samples is from Tables 1–3. **(B)** Focus on area with trace element data from plot **(A)**.

terion is ambiguous as it is not always detectable in synthetic corundum and sometimes can even be found in natural blue sapphire (Sorokina et al., 2019). Therefore, solely relying on LA-ICP-MS trace element analysis for distinguishing between natural and synthetic corundum origins, especially when grown by the hydrothermal method, can lead to misidentifications.

4.2 SIMS oxygen isotope discrimination

4.2.1 HT-treated and Be-diffused corundum

Results of high-spatial-resolution SIMS $\delta^{18}O$ measurements for HT-treated corundum in a non-controlled atmosphere (air) are indistinguishable between original and treated parts of the stone.

Corundum treated by the Be diffusion method shows both positive ($+12.81 \pm 0.12$ ‰ to $+13.21 \pm 0.12$ ‰) and negative oxygen isotope compositions (lower limit at -0.90 ± 0.13 (see Fig. 6)). However, the $\delta^{18}O$ mapping of one Be-diffused grain of metamorphic origin (sample no. 1), which shows a strong colour zonation, indicates a minor but significant increase in $\delta^{18}O$ in the outer ~ 0.5 mm, where $\delta^{18}O$ values are elevated by ~ 0.5 ‰. The untreated counterpart lacks similar increases along the corresponding margin, supporting the fact that enrichment is not an original $\delta^{18}O$ zonation and instead was caused by the oxygen isotopic exchange during the diffusion process. The geometry of the domain with elevated $\delta^{18}O$ is irregular and not always parallel to the margin. Moreover, the highest values are not directly at the margin, which is evidence against diffusion across the grain boundary as the main control on the $\delta^{18}O$ distribution. Regardless of the isotopic exchange mechanism, the minor change relative to the original $\delta^{18}O$ values would not affect the attribution to a potential source. Therefore, available data for Be-diffused corundum specimens from the gem market suggest that their $\delta^{18}O$ values likely reflect their original source composition. Regarding the possible source of material with slightly negative oxygen isotope compositions of up to -0.85 ‰, there are known deposits with corundum containing moderately depleted oxygen isotopic composition relative to SMOW. One of them is Ilakaka in Madagascar, and the others are from the Kola Peninsula (see Giuliani et al., 2014). Since the last occurrences are non-gem quality, the only commercial deposit is Ilakaka, with reported $\delta^{18}O$ values down to approximately -1 ‰, which is likely the source of Be-diffused stones analysed in this research.

4.2.2 Hydrothermally synthesized corundum

Analyses of all studied synthetic stones grown by the hydrothermal method show unusually negative oxygen isotope compositions varying from -7.84 ± 0.13 ‰ to -14.54 ± 0.13 ‰ (Fig. 7). Such unusual negative $\delta^{18}O$ values are likely to be due to the water used for the synthesis. The method itself is based on the synthesis of corundum in autoclaves with using local water as a solvent. Most hydrothermally synthesized corundum is produced by the company Taurus, which is based in Novosibirsk (Russia). According to the Global Network of Isotopes in Precipitation (GNIP), Novosibirsk is situated in the area where annually averaged precipitation is depleted in $\delta^{18}O$ by -14 ‰ relative to SMOW (The Global Network of Isotopes in Precipitation (GNIP) Brochure, 2025). If the manufacturing process changes in the

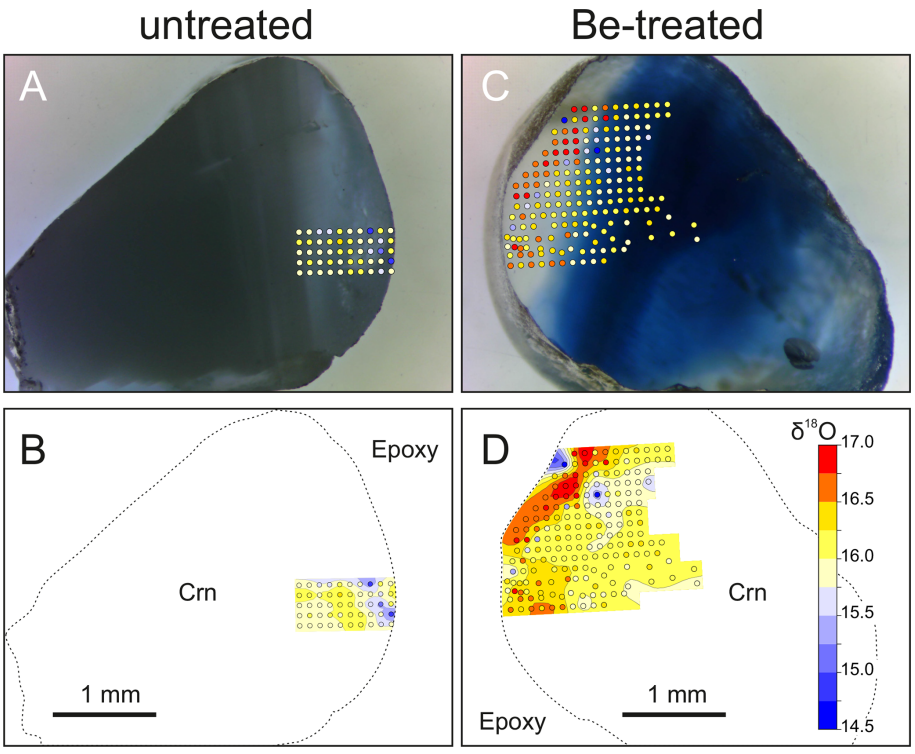

Figure 6. Photomicrographs **(A, C)** and SIMS δ^{18}O mapping **(B, D)** of sample no. 1 of metamorphic origin.

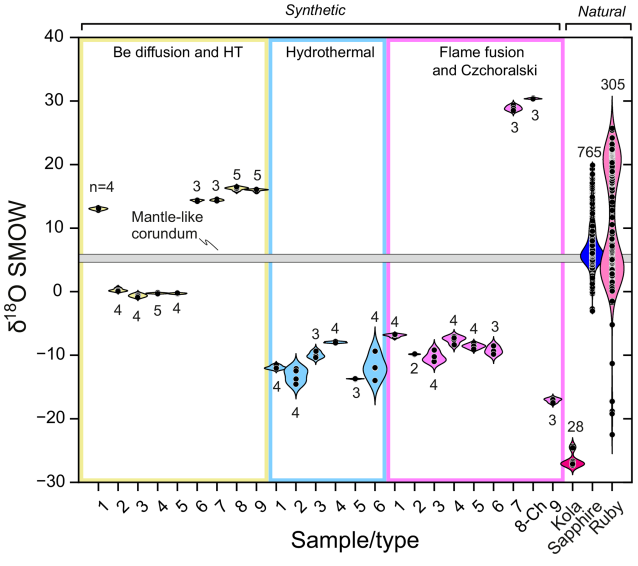

Figure 7. δ^{18}O values for HT-treated, Be diffusion, hydrothermal, and flame fusion corundum samples used in this study comparing to the literature data on 175 known ruby and sapphire deposits.

future by using water with a different δ^{18}O value, this would also affect δ^{18}O values of the synthesized corundum. However, for stones already on the market, the strongly depleted δ^{18}O values are characteristic of their origin.

Comparing the oxygen isotopic composition of hydrothermally synthesized corundum in our research with literature data, our results show more depleted δ^{18}O values (from -7.84 ± 0.13 ‰ to -14.54 ± 0.13 ‰) than those detected previously by Bidny et al. (2010) for hydrothermal corundum (from -0.7 ‰ to -5.8 ‰), which was analysed by laser fluorination oxygen isotope analysis consuming entire grain (Fig. 7). Our values are also uncommon for natural corundum, where the lowest δ^{18}O values vary from +23.5 ‰ (Giuliani et al., 2014) down to approximately -1.7 ‰ (Nigrozero in Karelia; Vysotskiy et al., 2014; Fig. 7). In this context, we note that the bulk δ^{18}O value of -5.2 ‰ determined for corundum from Nigrozero contrasts with core-to-rim analyses of this sample, which indicate limited variation with δ^{18}O values between -1.7 ‰ and -1.5 ‰ (Vysotskiy et al., 2014). Only the ruby deposit located in Khitostrov (Karelia, Russia) is known for its exotically depleted oxygen isotopic compositions. Our δ^{18}O analyses of corundum from this location average -26.51 ‰ (Fig. 7), which is slightly lower than δ^{18}O values by Bindeman and Serebryakov (2011; -18.65 to -25.96 ‰) and by Vysotskiy et al. (2014; -22.5 ‰). Vysotskiy et al. (2014) also reported δ^{18}O values of -17.2 for corundum from plagioclasite in Varatskoye of Karelia; however, they analysed grains in bulk, which can easily be contaminated by matrix minerals, and, therefore, these data are not further considered in this discussion. The unusually depleted oxygen isotopic content of Khitostrov corundum is likely due to the alteration of the

protolith by glacial meltwater during the ca. 2.4–2.3 Ga Paleoproterozoic "Slushball" glaciation (Bindeman and Serebryakov, 2011). In any case, the isotopic composition of corundum from the Khitostrov deposit obtained here and by other researchers is beyond the range we detected for hydrothermally synthesized corundum (-7.84 ± 0.13 ‰ to -14.54 ± 0.13 ‰). Because of the clear separation of high-spatial-resolution δ^{18}O SIMS analyses for hydrothermal and natural corundum, this method has the potential to distinguish between synthetic corundum and their natural analogues. It is further expected that the absolute δ^{18}O values of hydrothermally synthesized corundum will reflect the composition of water and other oxygen-bearing chemicals used during synthesis, thus potentially revealing further details on synthetic gem origins.

4.2.3 Flame fusion and Czochralski-grown corundum

Results obtained here also show negative δ^{18}O values from -6.73 ± 0.13 ‰ to -17.46 ± 0.13 ‰ for sapphires of blue, yellow, and orange colour grown by the flame fusion method. On the other hand, red-coloured (ruby) synthetic crystals grown by this method are characterized by strongly positive values of δ^{18}O from $+28.51 \pm 0.11$ ‰ to $+30.47 \pm 0.10$ ‰. Pomian-Srzednicki (1997) also detected negative δ^{18}O values for flame fusion sapphires of blue colour varying from -4.7 to -5.4 ‰, whereas red-coloured material grown by this method yielded positive values between $+11.6$ and $+30.4$ ‰ (Fig. 7; Pomian-Srzednicki, 1997). The process of flame fusion corundum synthesis occurs due to melting of aluminium oxide powder up to 2050 °C in a non-controlled atmosphere. Therefore, the reasons for such a strong isotopic dispersion from strongly negative (-17.46 ‰) to highly positive ($+30.47$ ‰) δ^{18}O values in flame fusion corundum can be explained by several factors (Pomian-Srzednicki, 1997; Pack, 2021): (1) derivation of alumina applied for the synthesis from different sources; (2) addition of oxides causing corundum colouration; (3) multiple processing steps for alumina, which, collectively, can strongly modify its original oxygen isotopic composition; and (4) processing and post-processing isotopic exchange with air (i.e. interaction of alumina with the oxyhydrogen flame and interaction with air during crystallization).

As can be seen from the discussion above, negative and positive δ^{18}O values obtained for flame fusion corundum are atypical for natural analogues falling primarily within a δ^{18}O range from -1.7 ‰ to $+23$ ‰, excluding the extremely depleted Khitostrov corundum (see the section above: "Hydrothermally synthesized corundum"). Therefore, such elevated values for flame fusion corundum are also atypical for their natural analogues. Intriguingly, Pack (2021) has proposed a method to identify flame fusion synthesis by Δ^{17}O analysis, a parameter for mass-independent isotope fractionation. In the data of Pack (2021), flame fusion synthetic corundum displays significantly lower Δ^{17}O from -0.239 to -0.533 compared to the natural counterparts, with a minimum value of -0.082. These Δ^{17}O anomalies appear to be due to isotopic exchange of the flux with the technical-grade O_2 prepared by liquefaction from air (Pack, 2021). In the future, Δ^{17}O analysis by SIMS (Schmidt et al., 2024) could be utilized as a less destructive technique compared to the laser fluorination method applied by Pack (2021).

4.2.4 Flux-grown corundum material

Previous studies also presented data on δ^{18}O compositions of flux-grown synthetic corundum by different manufactures. Pomian-Srzednicki (1997) measured corundum from Knischka (Austria), Chatham Gem Created (USA), Douros O.E. Created Gems (Greece), and Ramaura Cultured Rubies (USA). Obtained values varied from -0.2 ‰ to $+20.0$ ‰ of δ^{18}O (Pomian-Srzednicki, 1997). Bidny et al. (2010) reported results from measuring synthetic crystals originating from Kashan, Ramaura, and Crystal Growth Laboratory (MSU), which varied from $+4.8$ ‰ to 14.8 ‰ in δ^{18}O. The results of both studies (δ^{18}O $= -0.2$ ‰ to $+20.0$ ‰) fall in the range of δ^{18}O values between -1.7 ‰ and $+23$ ‰, which are characteristic for naturally occurring rubies and sapphires (Giuliani et al., 2014; Vysotskiy et al., 2014). Therefore, δ^{18}O analysis will not be able to discriminate synthetic flux-grown materials from their natural counterparts. However, the high temperature of flux corundum may also impart a mass-independent Δ^{17}O signature due to exchange with laboratory air so that a modified version of the method of Pack (2021) using high-spatial-resolution SIMS analysis may also be applied to identify flux-grown corundum in the future.

5 Conclusion

1. Solely relying on LA-ICP-MS trace element analysis for differentiation between natural and synthetic corundum origins, especially when grown by the hydrothermal method, can lead to misidentifications.

2. The results of high-spatial-resolution SIMS δ^{18}O measurements for HT-treated and Be-diffused corundum are largely indistinguishable between the original and treated parts of the stone.

3. The high spatial resolution of the SIMS δ^{18}O analysis of hydrothermally synthesized corundum yielded values between -7.84 ± 0.13 ‰ and -14.54 ± 0.13 ‰, which are atypical for natural corundum.

4. Equivalent data for flame fusion corundum are in the range of -6.73 ± 0.13 ‰ to -17.46 ± 0.13 ‰ for sapphires of blue, yellow, and orange colour and $+28.51 \pm 0.11$ ‰ to $+30.47 \pm 0.10$ ‰ for ruby; these are, again, atypical for natural corundum.

5. SIMS $\delta^{18}O$ analysis of corundum has strong potential to distinguish synthetic and natural counterparts at minimal sample consumption. Additional methods that are applicable for the differentiation of flame fusion corundum material include SIMS $\Delta^{17}O$ analysis; further research is required to test if negative mass-independent anomalies of up to $-0.5\,‰$ (Pack, 2021) can be routinely identified.

Data availability. No data sets were used in this article.

Author contributions. ESS and TH formulated the ideas and designed the experiments. AS designed the experiments for part of research. AS and JH carried out the experiments. TH provided the materials for the research. ESS, AS, and TH obtained funding for the research. ESS prepared the paper with all of the co-authors. AS prepared half of the original figures. AS, TH, and JH did a critical review of the paper and edited it.

Competing interests. The contact author has declared that none of the authors has any competing interests.

Disclaimer. Publisher's note: Copernicus Publications remains neutral with regard to jurisdictional claims made in the text, published maps, institutional affiliations, or any other geographical representation in this paper. The authors bear the ultimate responsibility for providing appropriate place names. Views expressed in the text are those of the authors and do not necessarily reflect the views of the publisher.

Acknowledgements. The authors are thankful to their colleagues from University Mainz (Roman Botcharnikov, Regina Mertz-Kraus, Stephan Buhre), University Heidelberg (Thomas Ludwig, Mario Trieloff), and Bhuwadol Wanthanachaisaeng from the Gem and Jewelry Research and Development Department (GIT).

Financial support. The work was carried out within the state assignment of the Vernadsky Institute of Geochemistry and Analytical Chemistry of the Russian Academy of Sciences (GEOKHI RAS), the group Geomaterial- und Gemstone research, University Mainz, the Institute for Gemstone research, Idar-Oberstein, and NCRIS via AuScope. The results on the identification of natural and synthetic corundum using oxygen isotopic analysis were patented under patent no. RU 2854293 (Elena S. Sorokina).

This open-access publication was funded
by Johannes Gutenberg University Mainz.

Review statement. This paper was edited by Pierre Lanari and reviewed by Laure Martin and one anonymous referee.

References

Baertschi, P.: Absolute ^{18}O content of Standard Mean Ocean Water, Earth Planet. Sci. Lett., 31, 341–344, https://doi.org/10.1016/0012-821X(76)90115-1, 1976.

Bidny, A. S., Dolgova, O. S., Baksheev, I. A., and Ekimenkova, I. A.: New data for distinguishing between hydrothermal synthetic, flux synthetic and natural corundum, J. Gemmol., 32, 7–13, https://doi.org/10.15506/JoG.2010.32.1-4.7, 2010.

Bindeman, I. N. and Serebryakov, N. S.: Geology, Petrology and O and H isotope geochemistry of remarkably ^{18}O depleted Paleoproterozoic rocks of the Belomorian Belt, Karelia, Russia, attributed to global glaciation 2.4 Ga, Earth Planet. Sc. Lett., 306, 163–174, https://doi.org/10.1016/j.epsl.2011.03.031, 2011.

Breeding, Ch. M., Shen, A. H., Eaton-Magaña, S., Rossman, G. R., Shigley, J. E., and Gilbertson, A.: Developments in gemstone analysis techniques and instrumentation during the 2000s, Gems Gemol., 46, 241–257, 2010.

Filina, M. I., Sorokina, E. S., Botcharnikov, R., Karampelas, S., Rassomakhin, M. A., Kononkova, N. N., Nikolaev, A. G., Berndt, J., and Hofmeister, W.: Corundum Anorthosites-Kyshtymites from the South Urals, Russia: A Combined Mineralogical, Geochemical, and U-Pb Zircon Geochronological Study, Minerals, 9, 234, https://doi.org/10.3390/min9040234, 2019.

Giuliani, G. and Groat, L. A.: Geology of corundum and emerald gem deposits: a review, Gems Gemol., 55, 464–489, https://doi.org/10.5741/GemS.55.4.464, 2019.

Giuliani, G., Christian, F. L., Cheilletz, A., Coget, P., Branquet, Y., and Laumonier, B.: Sulphate reduction by organic matter in Colombian emerald deposits: Chemical and stable isotope (C, O, H) evidence, Econ. Geol., 95, 5, 1129–1153, https://doi.org/10.2113/gsecongeo.95.5.1129, 2000.

Giuliani, G., Ohnenstetter, D., Fallick, A. E., Groat, L. A., and Fagan, A. J.: The geology and genesis of gem corundum deposits, in: Geology of Gem Deposits, 2nd edn., edited by: Groat, L. A., Mineralogical Association of Canada, Short Course Series 44, 29–112, https://doi.org/10.3749/9780921294696.ch02, 2014.

Gubelin, E. J. and Koivula, J. I.: Photoatlas of inclusions in gemstones, ABC Edition, Zurich, 532 pp., 1997.

Hughes, R. W.: Ruby and sapphire: a gemologist's guide, RWH Publishing/Lotus Publishing, 816 pp., 2017.

Jochum, K. P., Nohl, U., Herwig, K., Lammel, E., Stoll, B., and Hofmann, A. W.: GeoReM: a new geochemical database for reference materials and isotopic standards, Geostand. Geoanalytical Res., 29, 333–338, https://doi.org/10.1111/j.1751-08X.2005.tb00904.x, 2005.

Jochum, K. P., Weis, U., Stoll, B., Kuzmin, D., Yang, Q., Raczek, I., Jacob, D. E., Stracke, A., Birbaum, K., Frick, D. A., Günther, D., and Enzweiler, J.: Determination of reference values for NIST SRM 610-617 glasses following ISO Guidelines. Geostand. Geoanalytical Res., 35, 397–429, https://doi.org/10.1111/j.1751-908X.2011.00120.x, 2011.

Li, X. H. and Li, Q. L.: Major advances in microbeam analytical techniques and their applications in Earth Science, Sci. Bull., 61, 1785–1787, https://doi.org/10.1007/s11434-016-1197-5, 2016.

Liu, Z., Lin, J., Jiang, X., Zhu, X., Liu, W., Liu, Y., Zhang, W., and Hu, Z.: First attempt to determine oxygen isotopes in oxygen by MC-ICP-MS, J. Anal. At. Spectrom., 40, 1192–1202, https://doi.org/10.1039/D5JA00025D, 2025.

Muhlmeister, S., Fritsch, E., Shigley, J. E., Devouard, B., and Laurs, B. M.: Separating natural and synthetic rubies on the basis of trace-element chemistry, Gems Gemol., 34, 80–101, 1998.

Pack, A.: Isotopic Traces of Atmospheric O_2 in Rocks, Minerals, and Melts, Rev. Mineral. Geochem., 86, 217–240, https://doi.org/10.2138/rmg.2021.86.07, 2021.

Palke, A. C. and Shigley, J. E.: Laboratory Growth of Gem Materials and the Attempt to Replicate Nature, Gems Gemol., 60, 238–251, 2024.

Palke, A. C., Wong, J., Verdel, C., and Avila, J. N.: A common origin for Thai/Cambodian rubies and blue and violet sapphires from Yogo Gulch, Montana, USA?, Am. Mineral., 103, 469–479, https://doi.org/10.2138/am-2018-6164, 2018.

Peucat, J. J., Ruffault, P., Fritsch, E., Bouhnik-Le Coz, M., Simonet, C., and Lasnier, B.: Ga/Mg ratios as a new geochemical tool to differentiate magmatic from metamorphic blue sapphires, Lithos, 98, 261–274, https://doi.org/10.1016/j.lithos.2007.05.001, 2007.

Pomian-Srzednicki, I.: Caractérisation des corindons par mesure du rapport isotopique de l'oxygène $^{16}O/^{18}O$, Diploma work, Université de Lausanne, Institut de Minéralogie et Pétrographie, 94 pp., 1997.

Schmetzer, K. and Peretti, A.: Some Diagnostic Features of Russian Hydrothermal Synthetic Rubies and Sapphires, Gems Gemol., 35, 17–28, 1999.

Schmidt, S., Hertwig, A., Schmitt, A., Cionoiu, K., McKeegan, K., Bindeman, I., Pack, A., and Rocco, T.: A corundum reference material for oxygen isotope analysis by secondary ionization mass spectrometry, J. Anal. At. Spectrom., 39, 439–446, https://doi.org/10.1039/D3JA00229B, 2024.

Sorokina, E. S., Rassomakhin, M. ., Nikandrov, S. N., Karampelas, S., Kononkova, N. N., Nikolaev, A. G., Anosova, M. O., Somsikova, A. V., Kostitsyn, Y. A., and Kotlyarov, V. A.: Origin of Blue Sapphire in Newly Discovered Spinel–Chlorite–Muscovite Rocks within Meta-Ultramafites of Ilmen Mountains, South Urals of Russia: Evidence from Mineralogy, Geochemistry, Rb-Sr and Sm-Nd Isotopic Data, Minerals, 9, 36, https://doi.org/10.3390/min9010036, 2019.

Sorokina, E. S., Botcharnikov, R. E., Kostitsyn, Yu. A., Rösel, D., Häger, T., Rassomakhin, M. A., Kononkova, N. N., Somsikova, A. V., Berndt, J., Ludwig, Th., Medvedeva, E. V., and Hofmeister, W.: Sapphire-bearing magmatic rocks trace the boundary between paleo-continents: A case study of Ilmenogorsky alkaline complex, Uralian collision zone of Russia, Gondwana Res., 92, 239–252, https://doi.org/10.1016/j.gr.2021.01.001, 2021.

Sutherland, F. L., Zaw, K., Meffre, S., Thompson, J., Goemann, K., Thu, K., Nu, T. T., Zin, M. M., and Harris, S. J.: Diversity in Ruby Geochemistry and Its Inclusions: Intra- and Inter-Continental Comparisons from Myanmar and Eastern Australia, Minerals, 9, 28, https://doi.org/10.3390/min9010028, 2009.

The Global Network of Isotopes in Precipitation (GNIP) Brochure: http://www.iaea.org/services/networks/gnip (last access: March 2026), 2025.

Trail, D., Mojzsis, S. J., Harrison, T. M., Schmitt, A. K., Watson, E. B., and Young, E. D.: Constraints on Hadean zircon protoliths from oxygen isotopes, Ti-thermometry, and rare earth elements, Geochem. Geophys. Geosyst., 8, 1–22, 2007.

Vysotskiy, S. V., Ignat'ev, A. V., Levitskii, V. I., Nechaev, V. P., Velivetskaya, T. A., and Yakovenko V. V.: Geochemistry of stable oxygen and hydrogen isotopes in minerals and corundum-bearing rocks in northern Karelia as an indicator of their unusual genesis, Geochem. Int., 52, 773–782, https://doi.org/10.1134/S0016702914090109, 2014.

Wang, H., Cartier, L., Baumgartner, L., Bouvier, A.-S., Bégué, F., Chalain, J.-P., and Krzemnicki, M.: A Preliminary SIMS Study Using Carbon Isotopes to Separate Natural from Synthetic Diamonds, J. Gemmol., 36, 38–43, https://doi.org/10.15506/JoG.2018.36.1.38, 2018.

Wiedenbeck, M., Hanchar, J. M., Peck, W. H., Sylvester, P., Valley, J., Whitehouse, M., Kronz, A., Morishita, Y., Nasdala, L., Fiebig, J., and Franchi, I.: Further characterisation of the 91500 zircon crystal, Geostand. Geoanalytical Res., 28, 9–39, https://doi.org/10.1111/j.1751-908X.2004.tb01041.x, 2004.

Wong, J. and Verdel, C.: Tectonic environments of sapphire and ruby revealed by a global oxygen isotope compilation, Int. Geol. Rev., 60, 188–195, https://doi.org/10.1080/00206814.2017.1327373, 2017.